# Thermionic phenomena in a nanoscale ring without carrier reservoirs: A thermionic couple

Magnus Larsson,[1] A. G. Mal'shukov,[2] and K. A. Chao[1]
[1]*Division of Solid State Theory, Department of Physics, Lund University, S-223 62 Lund, Sweden*
[2]*Institute of Spectroscopy, Russian Academy of Science, 142190 Troitsk, Moscow oblast, Russia*
(Received 23 June 2004; revised manuscript received 7 September 2004; published 29 December 2004)

We have studied various thermionic processes in a small one-dimensional ring consisting of a metallic wire and an insulator which serves as the potential barrier for the charge carriers in the metallic wire. The ring is not connected to any particle reservoir, but at the two junctions it is attached to two phonon reservoirs with different temperatures. The lengths of both the metallic wire and the insulating part are shorter than the carrier mean free path, and therefore the nonequilibrium electron distribution function was solved using the Boltzmann-equation approach with electron-phonon interaction at the two junctions. We found that there is always a heat current flowing from the hot junction to the cold one. The electric current over the potential barrier increases monotonically as the Fermi energy in the metallic wire approaches the potential barrier height from below. Using a modulation doped semiconductor ring for numerical calculation, the thermionic current is found to be almost linear with respect to the temperature difference between the two junctions. Consequently, our system can be developed into a nanometer scale thermionic couple.

DOI: 10.1103/PhysRevB.70.235339 PACS number(s): 73.23.Ad, 72.15.Jf, 05.60.Gg

## I. INTRODUCTION

To study a materials transport properties, either electric conductivity, thermal conductivity, or thermoelectric phenomena, a sample is usually connected to two reservoirs with a voltage difference and/or a temperature difference. In recent years, because of the advancement of material fabrication and measurement technique, it is not unreasonable to expect the possibility to experimentally investigate the transport properties in a closed system without connecting to carrier reservoirs. Whether such experiments can be done in the near future or not, the topic itself is an interesting and challenging problem for the fundamental theory of transport in nonequilibrium systems. In this paper, we will analyze the thermionic processes in a small ring which is not connected to carrier reservoirs.

The thermoelectric effect has been extensively studied for many years, and the required breakthrough is in its efficiency. Since thermoelectric transport is a diffusive process, thermionic transport, which is based on a ballistic process of Richardson current[1] over a potential barrier, has been a fashionable research topic in the last ten years. In the earlier works on thermionic devices, there was the problem of charge carriers in the vacuum gap between two conductors.[2,3] To avoid this problem, structures of semiconductor superlattices[4] and metal-semiconductor multilayers[5] were proposed with the idea to replace the vacuum potential barrier by a semiconductor potential barrier. However, as long as there exists uncompensated charge, carriers can still accumulate in the semiconductor barrier region.[6] The physical significance of the potential barrier width for the thermionic transport in semiconductor superlattices was clarified recently,[7] where the calculated barrier strength for maximum thermionic efficiency agrees with the experimental observation.[8]

It was discovered[7] that for thermoelectric transport, the role of the width of potential barrier in a multilayers thermionic system is equivalent to the role of carrier mean free path in a thermoelectric system. In high quality doped semiconductor, the carrier mean free path can be much longer than the barrier width in typical semiconductor superlattices. Hence, the observed higher value of figure of merit of semiconductor superlattices with thermionic transport is most likely due to both their much lower value of thermal conductivity[9–11] and the possible hopping of carriers over several barrier wells. In this case, a relevant topic to be considered is the ballistic transport of a carrier through two wells with one barrier sandwiched in between. To simplify the problem, one can consider the thermionic process in a single-barrier system, in which the length of each lead is shorter than the mean free path. A lead of so short length cannot serve as a reservoir. It is then feasible to join the two leads to form a closed system in which the typical length is shorter than the carrier mean free path. Assuming that thermionic transport can be induced in such a system in a suitable way, then we have a thermionic phenomena in a nonequilibrium system. This problem will be studied in the present paper. We should mention that thermionic processes in a single barrier system connected to two carrier reservoirs was investigated earlier.[12,13]

The one-dimensional closed system to be studied is shown schematically in Fig. 1, where the $x$ axis is along the ring in clockwise direction. The ring system consists of a conducting wire [light shaded region marked with (c)] and an insulating wire [dark shaded region marked with (b)]. The length of the conducting wire $L$ is shorter than the carrier mean free path, and the carrier transport in the wire is ballistic. The single barrier potential profile around the ring is plotted at the top in Fig. 1, with the Fermi energy marked as $\epsilon_F$. Around positions $x_1$ and $x_2$ we introduce two very narrow regions of width $L_{\mathrm{ph}}$ for local heating. In these two narrow regions of phonon sources, the phonon temperatures $T_1$ and $T_2$ are well defined. The electron-phonon interaction is then restricted to these two point contacts $x_1$ and $x_2$, which can be considered as heat reservoirs. There are several existing tech-

 

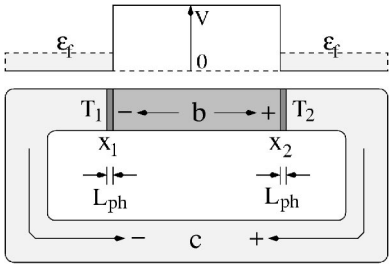


FIG. 1. A ring structure is schematically illustrated with a conducting channel [for example, an *n*-doped GaAs marked by (c)] and an insulating barrier (for example, an undoped $Al_xGa_{1-x}Al$ marked by (b)]. The two local phonon sources of narrow width $L_{ph}$ are set at positions $x_1$ and $x_2$ with respective temperatures $T_1$ and $T_2$. The potential profile around the ring is shown at the top of the figure with the Fermi energy $\epsilon_F$

niques which may be used here for local heating. We will return to this point later.

In Sec. II we will analyze the nonequilibrium carrier distribution functions. For small temperature difference $|T_1 - T_2|$ such that the terms of second order $[2|T_1-T_2|/(T_1 + T_2)]^2$ and higher can be neglected, a closed equation is obtained in Sec. III which provides a way to solve the nonequilibrium distribution functions numerically by iteration. Using the acoustic deformation potential for electron-phonon interaction which will be analyzed in Sec. IV, we study in Sec. V the thermionic current and the heat flow numerically in great detail. We notice that the sample structure shown in Fig. 1 is similar to a conventional thermoelectric couple. Consequently, in the concluding Sec. VI we will discuss the performance of our thermionic couple which may be a useful tool for investigating nanoscale thermal transport. Some remarks will be given at the last section.

## II. NONEQUILIBRIUM DISTRIBUTION FUNCTIONS

Although the length $L$ of the conducting wire (c) in Fig. 1 is shorter than the carrier mean free path, it can still be sufficiently long such that the carrier wave functions $\psi(x)$ are plane waves with wave vector $k$. We assume a very small cross-section of the conducting wire, and therefore only the lowest electron subband is populated. Hence the energy of the carrier is simply

$$\epsilon_k = \frac{\hbar^2 k^2}{2m^*} + U(x), \tag{1}$$

where $m^*$ is the carrier effective mass. The potential $U(x)$ is given by the top plot in Fig. 1. For the phonon part, in each of the two heat reservoirs at $x_1$ and $x_2$, the phonon source is specified by $\omega_q$. In the $l$th heat reservoir, the number of phonons $N_{q,l}$ is given by the Bose-Einstein function

$$N_{q,l} = [e^{(\hbar\omega_q/k_B T_l)} - 1]^{-1}, \tag{2}$$

where $l=1,2$.

The carrier temperature in our system and the corresponding nonequilibrium distribution function $f_k(x)$ remain to be determined. Since a charge carrier is scattered only locally at positions $x_1$ and $x_2$, its distribution function changes only at these scattering points. Hence, it is convenient to introduce two local distribution functions $f_k(x)=f_{k,c}$ in the conducting wire and $f_k(x)=f_{k,b}$ in the barrier region. At the scattering point $x_l$, the Boltzmann equation has the form

$$\frac{\hbar k}{m^* L}\frac{\partial f_k(x)}{\partial x} = I_{\rm coll}(l,k)\,\delta(x-x_l), \tag{3}$$

which is equivalent to

$$\frac{\hbar k}{m^* L}(f_{k,c} - f_{k,b}) = (-1)^l I_{\rm coll}(l,k), \tag{4}$$

where $I_{\rm coll}(k)$ is the carrier-phonon collision term.

We will derive the carrier-phonon collision terms with the Fermi golden rule for the absorption or emission of one phonon. To simplify the writing of the energy conservation for the scattering matrix element $W_{kk'}(q)$, we introduce the notations $\delta(kk'q)_\pm = \delta(\epsilon_k - \varepsilon_{k'} \pm \hbar\omega_q)$. We will specify each of the two distribution functions $f_{k,b}$ and $f_{k,c}$ explicitly in two different forms according to the direction of $k$ as illustrated in Fig. 1. For the plane wave traveling in clockwise direction, $k$ is positive and the distribution functions are $f_{k+,b}$ and $f_{k+,c}$. If $k$ is negative, the distribution functions are expressed as $f_{k-,b}$ and $f_{k-,c}$. Consequently, we will solve the four equations

$$\frac{\hbar k}{m^* L}(f_{k\pm,c} - f_{k\pm,b}) = (-1)^l I_{\rm coll}(l,k\pm). \tag{5}$$

Let us first describe all the scattering processes in the heat reservoir at position $x_1$ for a carrier moving in a clockwise direction. That is, we will first treat the equation

$$\frac{\hbar k}{m^* L}(f_{k+,b} - f_{k+,c}) = I_{\rm coll}(1,k+). \tag{6}$$

If the wave vector $k>0$ labels the final state of the carrier, then the scattering must be from an initial state with wave vector $k'$ into the final state with wave vector $k$ in the barrier region. There are four such scattering processes as shown in panels (1) and (2) in Fig. 2, two with phonon absorption (marked with "abs") and two with phonon emission (marked with "emi"). The probability for emitting or absorbing a phonon with $\omega_q$ contains a factor $(N_{q,1}+1)\delta(kk'q)_+$ for emission and $N_{q,1}\delta(kk'q)_-$ for absorption. The two processes in panel (1) have their initial states $k'-$ in the barrier region, and the two in panel (2) have their initial states $k'+$ in the conductor region. Taking into account the proper carrier occupation probabilities of the initial $k'\pm$ state and the final $k+$ state, the total contribution $I_{\rm in}(1,k+)$ to the collision term for scattering into the $k+$ state from all these four processes is

$$\begin{aligned} I_{\rm in}(1,k+) = \sum_{q,k'} W_{kk'}(q)\{&f_{k'+,c}(1-f_{k+,b}) \\ &\times[(N_{q,1}+1)\delta(kk'q)_+ + N_{q,1} \\ &\times\delta(kk'q)_-] + f_{k'-,b}(1-f_{k+,b}) \\ &\times[(N_{q,1}+1)\delta(kk'q)_+ + N_{q,1}\delta(kk'q)_-]\}. \end{aligned} \tag{7}$$

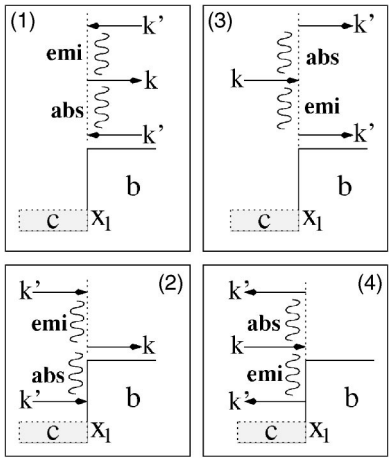


FIG. 2. Scattering processes for positive $k$ in the heat reservoir at position $x_1$. The wave vector $k$ labels the final states in panels (1) and (2), but the initial states in panels (3) and (4). The phonon absorption processes are marked with "abs," and the emission processes with "emi."

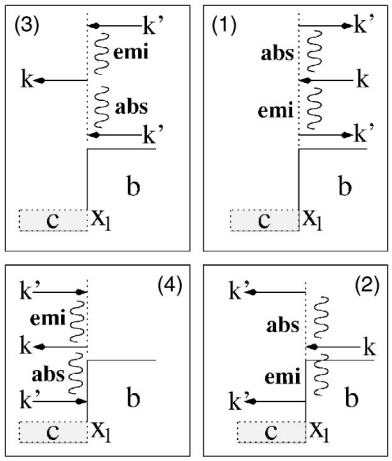


FIG. 3. Scattering processes for negative $k$ in the heat reservoir at position $x_1$. The wave vector $k$ labels the initial states in panels (1) and (2) and the final states in panels (3) and (4). The phonon absorption processes are marked with abs, and the emission processes with emi.

On the other hand, if the wave vector $k>0$ labels the initial state of the carrier, then the initial state must be in the conductor region. The final state with wave vector $k'$ can be either in the barrier region as shown in panel (3) or in the conductor region as shown in panel (4). Again, there are two phonon emission processes (marked with "emi") and two phonon absorption processes (marked with "abs"). Their contribution $I_{\text{out}}(1,k+)$ to the collision term for scattering out of the $k+$ state is then

$$I_{\text{out}}(1,k+) = \sum_{q,k'} W_{kk'}(q)\{f_{k+,c}(1-f_{k'+,b})[(N_{q,1}+1) \times \delta(kk'q)_- + N_{q,1}\delta(kk'q)_+] + f_{k+,c}(1-f_{k'-,c}) \times [(N_{q,1}+1)\delta(kk'q)_- + N_{q,1}\delta(kk'q)_+]\}. \quad (8)$$

The total scattering term $I_{\text{coll}}(1,k+)$ is simply $I_{\text{coll}}(1,k+) = I_{\text{in}}(1,k+) - I_{\text{out}}(1,k+)$ and Eq. (6) becomes

$$\frac{\hbar|k|}{m^*L}(f_{k+,b}-f_{k+,c}) = \sum_{q,k'} W_{kk'}(q) \times \{(1-f_{k+,b})(f_{k'+,c}+f_{k'-,b}) \times [(N_{q,1}+1)\delta(kk'q)_+ + N_{q,1}\delta(kk'q)_-] - f_{k+,c}(2-f_{k'+,b}-f_{k'-,c})[(N_{q,1}+1) \times \delta(kk'q)_- + N_{q,1}\delta(kk'q)_+]\}. \quad (9)$$

Next, we will treat the equation

$$\frac{\hbar k}{m^*L}(f_{k-,b}-f_{k-,c}) = I_{\text{coll}}(1,k-) \quad (10)$$

for a carrier moving in a counterclockwise direction with negative $k$. The four processes for scattering into the final state $k-$ are plotted in panels (3) and (4) in Fig. 3. Their contribution $I_{\text{in}}(1,k-)$ to the collision term for scattering into the final state $k-$ is

$$I_{\text{in}}(1,k-) = \sum_{q,k'} W_{kk'}(q)\{f_{k'+,c}(1-f_{k-,c})[(N_{q,1}+1) \times \delta(kk'q)_+ + N_{q,1}\delta(kk'q)_-] + f_{k'-,b}(1-f_{k-,c}) \times [(N_{q,1}+1)\delta(kk'q)_+ + N_{q,1}\delta(kk'q)_-]\}. \quad (11)$$

The scattering processes out of the initial state $k-$ are shown in panels (1) and (2) in Fig. 3, and their contribution $I_{\text{out}}(1,k-)$ to the collision term is

$$I_{\text{out}} = \sum_{q,k'} W_{kk'}(q)\{f_{k-,b}(1-f_{k'+,b})[(N_{q,1}+1) \times \delta(kk'q)_- + N_{q,1}\delta(kk'q)_+] + f_{k-,b}(1-f_{k'-,c}) \times [(N_{q,1}+1)\delta(kk'q)_- + N_{q,1}\delta(kk'q)_+]\}. \quad (12)$$

We notice that each panel in Fig. 3 can be obtained from the corresponding panel in Fig. 2 by reversing the directions of all $k$ and $k'$. The processes in Fig. 3 give the Boltzmann equation

$$\frac{\hbar|k|}{m^*L}(f_{k-,c}-f_{k-,b}) = \sum_{q,k'} W_{kk'}(q)\{(1-f_{k-,c})(f_{k'+,c}+f_{k'-,b}) \times [(N_{q,1}+1)\delta(kk'q)_+ + N_{q,1}\delta(kk'q)_-] - f_{k-,b}(2-f_{k'+,b}-f_{k'-,c})[(N_{q,1}+1) \times \delta(kk'q)_- + N_{q,1}\delta(kk'q)_+]\}. \quad (13)$$

We apply a similar analysis on the scattering processes in the heat reservoir around position $x_2$ to obtain two more Boltzmann equations

$$\frac{\hbar|k|}{m^* L}(f_{k+,c} - f_{k+,b}) = \sum_{q,k'} W_{kk'}(q)\{(1 - f_{k+,c})(f_{k'-,c} + f_{k'+,b}) \times[(N_{q,2} + 1)\delta(kk'q)_+ + N_{q,2}\delta(kk'q)_-] - f_{k+,b}(2 - f_{k'-,b} - f_{k'+,c})[(N_{q,2} + 1) \times \delta(kk'q)_- + N_{q,2}\delta(kk'q)_+]\} \quad (14)$$

and

$$\frac{\hbar|k|}{m^* L}(f_{k-,b} - f_{k-,c}) = \sum_{q,k'} W_{kk'}(q)\{(1 - f_{k-,b})(f_{k'-,c} + f_{k'+,b}) \times[(N_{q,2} + 1)\delta(kk'q)_+ + N_{q,2}\delta(kk'q)_-] - f_{k-,c}(2 - f_{k'-,b} - f_{k'+,c})[(N_{q,2} + 1) \times \delta(kk'q)_- + N_{q,2}\delta(kk'q)_+]\}. \quad (15)$$

The nonequilibrium distribution functions can be expressed in the general form

$$f_{k\pm,\alpha} = f_{0,\alpha}(\epsilon_k) + \delta f_{k\pm,\alpha}, \quad (16)$$

where $\alpha$ can be either $b$ or $c$. With a good choice of the equilibrium distribution functions $f_{0,b}(\epsilon_k)$ and $f_{0,c}(\epsilon_k)$, the correction terms $\delta f_{k\pm,\alpha}$ can be obtained by solving the above set of equations.

## III. SMALL TEMPERATURE DIFFERENCE

The set of Eqs. (9) and (13)–(15) are difficult to solve for the general case. Let us set $T_1 > T_2$ and define $\Delta T = T_1 - T_2$ and the lattice temperature $T_0 = (T_1 + T_2)/2$. We will consider a simpler situation such that terms of order $(\Delta T/T_0)^2$ and higher are small and can be neglected. To avoid ambiguity, we call such a situation small temperature difference. Hence, we have the equilibrium distribution

$$f_{0,b}(\epsilon_k) = f_{0,c}(\epsilon_k) = f_0(\epsilon_k) = [e^{(\epsilon_k - \mu)/k_B T_0} + 1]^{-1}. \quad (17)$$

We will further assume a weak interaction between the charge carriers and phonons. Under these conditions the correction terms $\delta f_{k\pm,\alpha}$ are small compared to $f_0(\epsilon_k)$. Under the condition of small temperature difference as defined above, we can approximate $N_{q,1} = N_{q,0} + \delta N_q$ and $N_{q,2} = N_{q,0} - \delta N_q$ well with

$$N_{q,0} = [e^{(\hbar\omega_q/k_B T_0)} - 1]^{-1}. \quad (18)$$

In the above approximation, $\delta N_q$ is linear in $\Delta T/T_0$. We will linearize Eqs. (9) and (13)–(15) with respect to the small quantities $\delta N_{q,l}$ and $\delta f_{k\pm,\alpha}$. In these four equations, each term on the right-hand side is a product of two electron distributions functions and one phonon distribution function. Hence, by linearizing these terms, each physical process includes four groups of terms; one group of terms is proportional to $\delta f(\epsilon_k)$, the other group proportional to $\delta N(\omega)$, the third group proportional to $\delta f(\epsilon_k + \hbar\omega)$, and the last group proportional to $\delta f(\epsilon_k - \hbar\omega)$. It is important to mention that the $\delta f(\epsilon_k + \hbar\omega)$ group contains phonon emission if $k$ is the wave vector of the final state, and phonon absorption if $k$ is the wave vector of the initial state. Similarly, the $\delta f(\epsilon_k - \hbar\omega)$ group contains phonon absorption if $k$ is the wave vector of the final state, and phonon emission if $k$ is the wave vector of the initial state. These emission and absorption processes can be easily recognized in Figs. 2 and 3.

After linearizing the four equations (9) and (13)–(15), there is a lengthy but trivial algebraic manipulation to combine various terms to simple forms. Then, using the phonon density of states $\rho(\omega)$ to convert the summation over $q$ into an integration over $\omega$, we arrive at a closed equation for

$$\delta f(\epsilon_k) = \delta f_{k+,c} - \delta f_{k-,c}. \quad (19)$$

If we set $k$ positive, this equation has the form

$$\frac{2\hbar k}{m^* L}\delta f(\epsilon_k) = \frac{L_{\rm ph}}{L}\int d\omega W(\omega)\rho(\omega)[A\delta f(\epsilon_k + \hbar\omega) + B\delta f(\epsilon_k - \hbar\omega) + C\delta f(\epsilon_k) + D\delta N(\omega)], \quad (20)$$

where $L_{\rm ph}$ is the width of each heat reservoir as indicated in Fig. 1. We define

$$F_\pm(\epsilon_k, \omega) = -f_0(\epsilon_k)[e^{(\epsilon_k \pm \hbar\omega - \epsilon_F)/k_B T_0} - 1]/\sqrt{\epsilon_k \pm \hbar\omega}, \quad (21)$$

$$G_\pm(\epsilon_k, \omega) = f_0(\epsilon_k \pm \hbar\omega)[e^{(\epsilon_k - \epsilon_F)/k_B T_0} - 1]/\sqrt{\epsilon_k \pm \hbar\omega}, \quad (22)$$

$$H_\pm(\epsilon_k, \omega) = 2f_0(\epsilon_k \pm \hbar\omega)[e^{(-\epsilon_k + \epsilon_F)/k_B T_0} + 1]^{-1}/\sqrt{\epsilon_k \pm \hbar\omega}, \quad (23)$$

$$N_0(T_e) = \int \rho(\omega)[e^{(\hbar\omega/k_B T_0)} - 1]^{-1} d\omega, \quad (24)$$

to express the functions $A$, $B$, $C$, and $D$ in compact forms

$$A = N_0(T_0)[1 + \Theta(\epsilon_k + \hbar\omega - V)]F_+(\epsilon_k, \omega), \quad (25)$$

$$B = [N_0(T_0) + 1][\Theta(\epsilon_k - \hbar\omega) + \Theta(\epsilon_k - \hbar\omega - V)]F_-(\epsilon_k, \omega), \quad (26)$$

$$C = [N_0(T_0) + 1][1 + \Theta(\epsilon_k + \hbar\omega - V)]G_+(\epsilon_k, \omega) + N_0(T_0) \times[\Theta(\epsilon_k - \hbar\omega) + \Theta(\epsilon_k - \hbar\omega - V)]G_-(\epsilon_k, \omega), \quad (27)$$

$$D = [1 + \Theta(\epsilon_k + \hbar\omega - V)]H_+(\epsilon_k, \omega)/N_0(T_0) - [\Theta(\epsilon_k - \hbar\omega) + \Theta(\epsilon_k - \hbar\omega - V)]H_-(\epsilon_k, \omega)/[N_0(T_0) + 1], \quad (28)$$

where $\Theta(E) = 1$ if $E > 0$ and $\Theta(E) = 0$ if $E < 0$. In the above equations, $V$ is the potential barrier height indicated in Fig. 1. As we will see later when we calculate the thermionic current, it is sufficient to know $\delta f(\epsilon_k)$ without the knowledge of individual $\delta f_{k\pm,\alpha}$.

## IV. ELECTRON-PHONON INTERACTION

To complete the theoretical analysis, we need to do more for the scattering between the carriers and phonons. Using the deformation potential approach, the scattering rate of one-dimensional electrons by three-dimensional acoustic

phonons in a quantum wire was derived earlier.[14,15] However, using this scattering rate for our system, it requires two modification. Since we have pointlike phonon sources the details of which are not specified, the form factor has a value between zero and 1. In our calculation we set the form factor equal to 1. Furthermore, since in our system electrons interact with phonons only in each heat reservoir of a narrow width $L_{\rm ph}$ instead of in the entire conducting wire of length $L$, the scattering rate derived in Ref. 14 should be scaled by a factor $L_{\rm ph}/L$. Then the electron-phonon scattering rate $1/\tau$ in our system can be expressed as

$$\frac{1}{\tau} = \frac{L_{\rm ph}}{L}\frac{1}{\tau_{\rm 1D}},$$

$$\frac{1}{\tau_{\rm 1D}} = \int d\omega W(\omega)\rho(\omega)\left[\frac{N_0(T_0)+1}{\sqrt{\epsilon_k-\hbar\omega}} + \frac{N_0(T_0)}{\sqrt{\epsilon_k+\hbar\omega}}\right], \quad (29)$$

where the scattering matrix element $W(\omega)$ calculated with the deformation potential is proportional to the frequency $\omega$.

We will use the Debye model for the acoustic phonons, which gives $\rho(\omega)\propto\omega^2$. Therefore, $W(\omega)\rho(\omega)=\mathcal{M}\omega^3$, where $\mathcal{M}$ contains the deformation potential constant and other material parameters, but is independent of the frequency $\omega$. We notice that the same product $W(\omega)\rho(\omega)$ appears in the integral in Eq. (20), as it should be because in both Eqs. (20) and (29) the dynamical mechanism is the electron-phonon interaction. By combining these two equations, we obtain for positive $k$

$$2\frac{\hbar k}{m^*}\delta f(\epsilon_k) = L_{\rm ph}\frac{1}{\tau_{\rm 1D}}\frac{\mathcal{P}(\epsilon_k)}{\mathcal{Q}(\epsilon_k)}, \quad (30)$$

with

$$\mathcal{P}(\epsilon_k) = \int_0^{\omega_D} d\omega\omega^3[A\delta f(\epsilon_k+\hbar\omega) + B\delta f(\epsilon_k-\hbar\omega) + C\delta f(\epsilon_k) + D\delta N(\omega)] \quad (31)$$

and

$$\mathcal{Q}(\epsilon_k) = \int_0^{\omega_D} d\omega\omega^3\left[\frac{N_0(T_0)+1}{\sqrt{\epsilon_k-\hbar\omega}} + \frac{N_0(T_0)}{\sqrt{\epsilon_k+\hbar\omega}}\right], \quad (32)$$

where $\omega_D$ is the Debye frequency. From the above three equations, the function $\delta f(\epsilon_k)$ can be calculated by numerical iteration.

## V. THERMIONIC CURRENT AND HEAT FLOW

To calculate the thermionic (electric) current over the barrier [region (b) in Fig. 1], we can use the distribution function either in the metallic wire [region (c) in Fig. 1] or in the barrier. This will give the same result because the current is continuous within the sample. For the convenience of analyzing the numerical results in a later section, we will define $e$ as the magnitude of the electron charge. If we use the distribution function in the metallic wire, the current can be expressed as

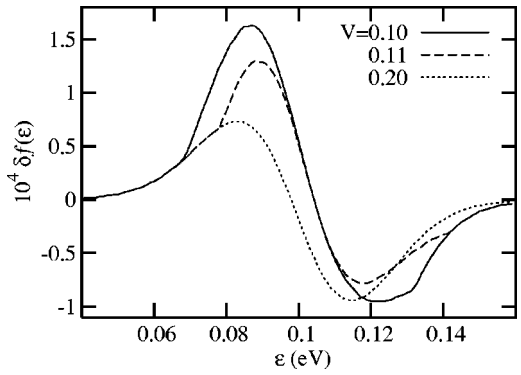


FIG. 4. $\delta f(\epsilon_k)$ calculated with Eqs. (30)–(32) for various values of barrier potential heights.

$$j = 2e\sum_{k>0}\frac{\hbar k}{m^* L}(f_{k+,c}-f_{k-,c}) = \frac{e}{\pi\hbar}\int_0^\infty d\epsilon(\delta f_{k+,c}-\delta f_{k-,c}). \quad (33)$$

On the other hand if we use the distribution function in the barrier region where the energy of the carrier must be larger than the barrier height $V$, the current is calculated with the integral

$$j = \frac{e}{\pi\hbar}\int_V^\infty d\epsilon(\delta f_{k+,b}-\delta f_{k-,b}). \quad (34)$$

Since we have already derived the formula to calculate $\delta f_{k+,c}-\delta f_{k-,c}=\delta f(\epsilon_k)$ [Eqs. (30)–(32), we will use Eq. (33) to obtain the current. However, to check that our linearized formulas are indeed correct and our numerical results are accurate enough, we have also used Eq. (34) to calculate the current and indeed obtain the same result.

For numerical calculation, we will consider a doped GaAs for the metallic wire and an $Al_xGa_{1-x}As$ for the barrier. The Fermi energy in the GaAs is set at 0.1 eV, which is the lower limit of the barrier height $V$, corresponding to the Al concentration about $x=0.12$. The Debye frequency for GaAs is $\hbar\omega_D=31.9$ meV, and from the calculations in Ref. 14 we estimate $\tau_{\rm 1D}=10^{-12}$ s. Each heat source is restricted in a narrow region of $L_{\rm ph}=100$ Å. The temperatures are chosen as $T_1=100$ K and $T_2=80$ K. The electron temperature in Eq. (17) is equal to the mean lattice temperature $T_0=(T_1+T_2)/2=90$ K. With such a choice of parameter values, the terms neglected are smaller than $(\Delta T/T_0)^2\simeq 0.05$. When we increase the value of $T_2$ to make $\Delta T$ smaller, there is no qualitative change of our numerical results. In fact, in Fig. 7 which will be presented later we have calculated the thermionic current for $\Delta T$ in a range from zero to 25 K. We will discuss this point further in the later section where we introduce the thermionic couple.

Equations (30)–(32) are solved numerically by iteration with initial input $\delta f(\epsilon_k+\hbar\omega)=0$ and $\delta f(\epsilon_k-\hbar\omega)=0$. In our convention, a positive current flows through the sample (Fig. 1) in clockwise direction. The self-consistent solution of $\delta f(\epsilon)$ is plotted in Fig. 4 for three values of barrier height $V=0.1$, 0.11, and 0.2 eV. Let us first analyze the case of high

potential barrier $V=0.2$ eV which is substantially high in the sense that $V-(\epsilon_F+\hbar\omega_D)\gg k_BT_0$. $\delta f(\epsilon)$ behaves smoothly and is positive for low $\epsilon$ but negative for high $\epsilon$. Hence, the low-energy electrons flow clockwise and the high-energy electrons flow counterclockwise. These two current components cancel each other exactly, and the integral of this curve, which is the thermionic current from Eq. (33), turns out to be zero. The absence of thermionic current can also be seen from Eq. (34), for which the integrand is practically zero for all $\epsilon>V$ as indicated in Fig. 4.

Even if there is no thermionic current, there exists a heat flow from the high-temperature region around $x_1$ to the low-temperature region around $x_2$. The heat current is calculated from

$$j^q=\frac{1}{\pi\hbar}\int_0^\infty d\epsilon(\epsilon-\epsilon_F)\delta f(\epsilon). \tag{35}$$

Because of the additional factor $\epsilon-\epsilon_F$, the integrand is always negative, implying a heat flow in the metallic wire from $x_1$ to $x_2$. The corresponding physical processes are low-energy (cold) electrons flow to $x_1$, where they absorb phonons, and high-energy (hot) electrons move to $x_2$, where they emit phonons. The net effect is the heat transfer in the metallic wire from the hot point to the cold point.

The $\theta$ functions in Eqs. (25)–(28) set several restrictions on the electron transport processes. The most important feature is the two energy thresholds at $V-\hbar\omega_D$ and $V+\hbar\omega_D$. If an electron in the metallic wire has energy $\epsilon<V-\hbar\omega_D$, it cannot absorb a phonon to get into the barrier region. Similarly, if an electron in the metallic wire has energy $\epsilon<V+\hbar\omega_D$, it cannot emit a phonon to get into the barrier region. For $V=0.2$ eV, the two thresholds $V-\hbar\omega_D=0.168$ eV and $V+\hbar\omega_D=0.232$ eV are outside the energy range in Fig. 4, where $\delta f(\epsilon)$ is already negligibly small. This is the reason why the corresponding curve is very smooth. For the two lower values of barrier potential $V=0.11$ and 0.1 eV, in each curve we see two kinks at energy $\epsilon=V\pm\hbar\omega_D$. Because we have ignored multiphonon processes in our theory, all curves in Fig. 4 merge into one another in both limits of large $\epsilon$ and small $\epsilon$.

We note that in Fig. 4, for each of the two curves with $V=0.11$ and 0.1 eV, the area under the positive $\delta f(\epsilon)$ in the low $\epsilon$ region is larger than the area above the negative $\delta f(\epsilon)$ in the high $\epsilon$ region. Consequently, more low-energy electrons absorb phonons around the high-temperature heat source and travel into the barrier in clockwise direction, and less high-energy electrons emit phonons around the low-temperature heat source and travel into the barrier in counterclockwise direction. This results in a positive thermionic current in the ring system, when calculated with Eq. (33).

Using the above procedure to calculate the thermionic current as a function of the barrier potential height $V>\epsilon_F$, the result is plotted in Fig. 5. The current has its maximum when the barrier height is equal to the Fermi energy $\epsilon_F=0.1$ eV, and decreases monotonically with increasing barrier potential. The current diminishes when $V-(\epsilon_F+\hbar\omega_D)$ becomes larger than $k_BT_0$.

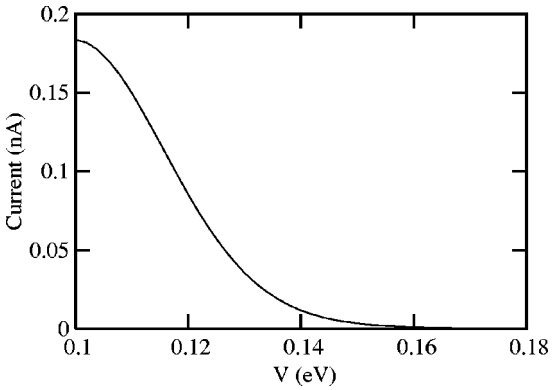


FIG. 5. Thermionic current as a function of barrier potential height for $\epsilon_F=0.1$ eV, $T_1=100$ K, and $T_2=80$ K.

We continue to calculate the heat current $j^q$ flowing in the metallic wire, using Eq. (35). This is shown in Fig. 6 as solid curve, which is negative because this heat flow is in a counterclockwise direction. The heat current through the barrier can be calculated similarly as

$$j^q=\frac{1}{\pi\hbar}\int_0^\infty d\epsilon(\epsilon-\epsilon_F)(\delta f_{k+,b}-\delta f_{k-,b}). \tag{36}$$

This heat flow is along the clockwise direction, and is plotted in Fig. 6 as the positive dashed curve. Both heat currents flow from the hot region to the cold region, and the amount of heat flow in the metallic wire is larger than that over the barrier, as expected. When the barrier height becomes larger than $\epsilon_F+\hbar\omega_D$, the heat flow over the barrier approaches zero rapidly, while the heat flow in the metallic wire remains almost constant. This is the situation we discussed earlier in connection to the barrier height $V=0.2$ eV. We should mention that we only need $\delta f_{k+,\alpha}-\delta f_{k-,\alpha}$ to calculate the thermionic current and the heat flow, although individual functions $\delta f_{k\pm,\alpha}$ can also be calculated.

## VI. THERMIONIC COUPLE

The sample structure shown in Fig. 1 is essentially a thermionic couple analogous to the conventional thermoelectric

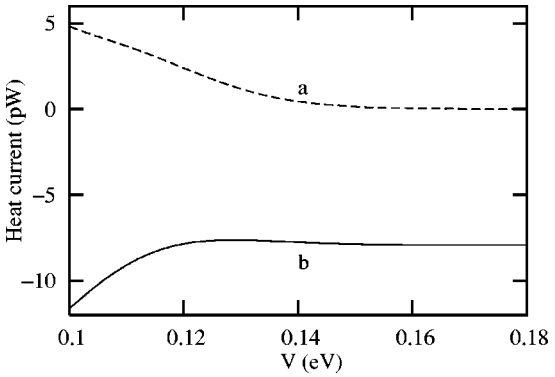


FIG. 6. Heat current as a function of barrier potential height, for $\epsilon_F=0.1$ eV, $T_1=100$ K, and $T_2=80$ K. Curve a is the heat flow over the barrier, and curve b is the heat flow through the metallic wire.

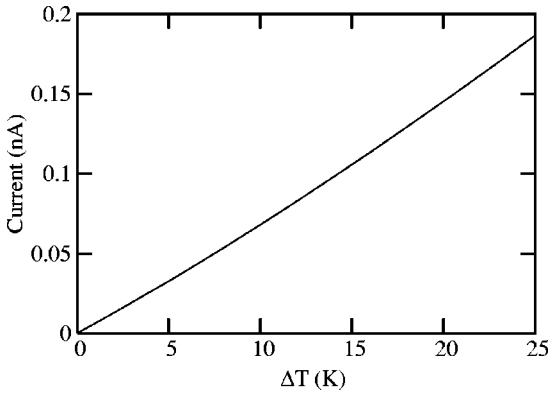


FIG. 7. Thermionic current over a barrier potential height $V=0.11$ eV as a function of the temperature difference $\Delta T=T_1-T_2$ with $T_2=77$ K.

couple made from two metals. Since local temperature measurement is important to nanoscale thermal transport,[16] it is then worthwhile to examine the performance of such a thermionic couple. We will first use the result in Fig. 5 to demonstrate the essential features of a thermionic couple. Since a thermionic couple measures the relative temperature $\Delta T$ just as a conventional thermoelectric couple does, we need a reference temperature for calibration. This reference temperature can be either $T_1$ or $T_2$, and we will use liquid nitrogen temperature as our reference temperature to set $T_2=77$ K. Then we have to determine the potential barrier height $V$ such that within the temperature range $\Delta T$ a sufficiently large thermionic current can be generated. From Fig. 5 we see that a barrier height $V=0.11$ eV will serve our purpose. For this thermionic couple with $\epsilon_F=0.1$ eV and $V=0.11$ eV, in Fig. 7 we show the thermionic current as a function of the temperature difference $\Delta T=T_1-T_2$ with $T_2=77$ K. It is interesting to notice that the current varies with $\Delta T$ almost linearly, which is the desired property for a practical thermocouple.

The thermionic current depends on the potential barrier height $V$, the Fermi energy $\epsilon_F$, as well as temperatures $T_1$ and $T_2$. Therefore, to make a thermionic couple with high efficiency in a particular temperature range requires the proper choice of these parameter values. For a given temperature $T$, the thermionic process is optimized with the condition[7] that the thermal energy $k_BT$ is about the same as the energy difference $V-\epsilon_F$. Consequently, to have a thermionic couple operated in the temperature range between $T_1$ and $T_2$, we should design a sample with $V-\epsilon_F$ comparable to $(T_1+T_2)/2$. For the thermionic couple shown in Fig. 7, which is designed to operate around the temperature 90 K, we have $(V-\epsilon_F)/k_B\simeq 120$ K. Of course, what we provide here is just a theoretical guideline. In reality, there are other possible material problems and engineering difficulties to overcome.

## VII. FINAL REMARKS

Before closing this paper, we should address the question of pointlike heat sources shown in Fig. 1. To our knowledge four methods of local heating exist. A pointlike source phonon cavity was used in the experiment to detect quantized thermal conductance.[17] With thermal excitation of impurity atoms by an electron current, under a nonequilibrium condition local phonons can be created.[18] This local heating technique was used to study electromigration in metal nanobridges.[19] Focused laser beam was also used to generate acoustic phonons in a localized region which depends on the size of the laser beam.[20] Finally, a local heat reservoir can be established by passing a current through a point contact. With this method the thermopower[21] as well as the Peltier coefficient and the thermal conductance[22] of a quantum point contact were investigated.

Whether some of these local heating methods can be applied directly to our system or need modification to fit into our sample structure, is outside the scope of the present work which is the first theoretical study on thermionic emission in a nanostructured material. However, we do realize one essential aspect as to the size of the local heat reservoir. In our numerical study we have set the size $L_{\rm ph}$ of our heat source at 10 nm. However, this is not the lower limit, because from Eq. (30) we see that an increase of $L_{\rm ph}$ will increase $\delta f(\epsilon_k)$ and will therefore enhance the thermionic current. The physical picture of this phenomenon is that in a larger heat source the more frequent electron-phonon scattering will increase the thermionic transport over the barrier. We should point out that an increase of $L_{\rm ph}$ has no influence on the ballistic transport both in the metallic wire and over the barrier. We should also point out that the possible multiple phonon scattering processes, which are not included in our theoretical analysis, may affect the final numerical results quantitatively but not qualitatively. Consequently, it is not unreasonable to expect the realization of a submicron heat source to be attached to our thermionic couple.

[1] S. M. Sze, *Physics of Semiconductor Devices*, 2nd ed. (Wiley, New York, 1981), Sec. 5.4.1.
[2] I. Langmuir, Phys. Rev. **21**, 419 (1923).
[3] G. D. Mahan, J. Appl. Phys. **76**, 4362 (1994).
[4] G. D. Mahan and J. O. Sofo, J. Appl. Phys. **83**, 4683 (1998).
[5] G. D. Mahan and L. M. Woods, Phys. Rev. Lett. **80**, 4016 (1998).
[6] G. D. Mahan, J. Appl. Phys. **87**, 7326 (2000).
[7] A. G. Mal'shukov, Zhongshui Ma, V. B. Antonyuk, and K. A. Chao, Solid State Commun. **119**, 563 (2001).
[8] R. Venkatasubramanian, E. Siivola, T. Colpitts, and B. O'Quinn, Nature (London) **413**, 597 (2001).
[9] T. Yao, Appl. Phys. Lett. **51**, 1798 (1987).
[10] S. M. Lee, D. G. Cahill, and R. Ventakasubramanian, Appl. Phys. Lett. **70**, 2957 (1997).
[11] G. Chen and M. Neagu, Appl. Phys. Lett. **71**, 2761 (1997).
[12] T. W. Hickmott, P. M. Solomon, R. Fischer, and H. Morkoc, J. Appl. Phys. **57**, 2844 (1985).
[13] A. Shakouri and J. E. Bowers, Appl. Phys. Lett. **71**, 1234 (1997);

A. Shakouri, C. LaBounty, J. Piprek, P. Abraham, and J. E. Bowers, *ibid.* **74**, 88 (1998).
[14] R. Mickevicius and V. Mitin, Phys. Rev. B **48**, 17 194 (1993).
[15] B. K. Ridley and N. A Zakhleniuk, J. Phys.: Condens. Matter **8**, 8525 (1996).
[16] D. G. Cahill, W. K. Ford, K. D. Goodson, G. D. Mahan, A. Majumdar, J. M. Humphrey, R. Merlin, and S. R. Phillpot, J. Appl. Phys. **93**, 793 (2003).
[17] K. Schwab, E. A. Henriksen, J. M. Worlock, and M. L. Roukes, Nature (London) **404**, 974 (2000).
[18] Z. Chen and R. S. Sorbello, Phys. Rev. B **47**, 13 527 (1993).
[19] K. S. Ralls, D. C. Ralph, and R. A. Buhrman, Phys. Rev. B **40**, 11 561 (1989).
[20] F. Dietzel and W. Dietsche, Phys. Rev. B **48**, 4713 (1993).
[21] L. W. Molenkamp, H. van Houten, C. W. J. Beenakker, C. T. Foxon, and R. Eppenga, Phys. Rev. Lett. **65**, 1052 (1990).
[22] L. W. Molenkamp, Th. Gravier, H. van Houten, O. J. A. Buijk, C. T. Foxon, and M. A. A. Mabesoone, Phys. Rev. Lett. **68**, 3765 (1992).